ACADEMIC JOURNALS
expand your knowledge

Journal of Mechanical Engineering Research

Full Length Research Paper

Peristaltic transport of a second-grade dusty fluid in a tube

H. Tariq[1,2] and A. A. Khan[2]*

[1]Department of Mathematics and Statistics, International Islamic University Islamabad, 44000, Pakistan.
[2]Department of Mathematics, National University of Modern Languages Islamabad, Pakistan.

These article intents to analyze the behavior of second-grade dusty fluid flowing through a flexible tube whose walls are induced by the peristaltic movement. Coupled equations for the fluid and solid particles have been modelled by considering streamline conversions. Regular perturbation technique has been implemented to get the solutions and the outcomes are demonstrated through graphs. The impact of diverse parameters on the contour presentations and on the velocity of the solid grains and fluid has been illustrated. The velocity for both fluid and solid grains is increased with the enhancement in wave number and Reynolds number. In retrograde region, pumping rate increases with the increase in α and it decreases for increased values of δ.

Key words: Peristaltic flow, second-grade dusty fluid, tube, axisymmetric flow.

INTRODUCTION

The flow in a flexible tube is induced by progressive wave along its walls. This progressive wave phenomenon is known as peristalsis. The particular application of peristalsis in an elastic tube is found in many biological systems such as cardiovascular system, fertile egg in the female fallopian tube, trachea and duodenum. The mechanism of peristalsis was first modelled by assuming long wavelength analysis along with low Reynolds number. Morgan and Kiely (1957) investigated the propagation of a harmonic wave in a flexible tube. Womersley (1957) considered the axisymmetric flow in a tube. Singh and Singh (2014) considered the Rabinowitsch fluid model in a tube. Hameed et al. (2015) considered the fractional second-grade fluid in a tube. Shaheen and Asjad (2018) presented a study that deals with the convectively heated surface of the tube. The fluid

that they assumed in this study was Sisko fluid. There after theories were expanded to non-creeping flow. Yin and Fung (1969) studied the peristaltic movement in a tube. Streeter et al. (1964) investigated the non-creeping flow in an arterial system of a dog. Olsen and Shapiro (1967) studied the unsteady movement in a tube which was elastic. In a tube, the second order fluid was studied by Siddiqui and Schwarz (1994). Pandey and Claube (2010) considered the creeping and non-creeping movement of the fluids which were viscoelastic in nature and flowing in a tube which was non-uniform. A recent study that deals with the non-creeping flow is presented by (Pantokratoras, 2018; Hayat et al., 2016a, b, 2017a, b, c, 2018, 2019, 2018a, b, 2017b; Khan et al., 2017, 2018a, b, 2019; Rashid et al., 2019; Qayyum et al., 2018a, b; Asghar et al.,2018, 2019a, b, 2019c, 2020a, b;

*Corresponding author. E-mail: ambreen.afsar@iiu.edu.pk.

Javid et al., 2019a, b; Ali et al., 2019b; Dogonchi et al., 2020) are notable researches in the same context.

It is pertinent to mention here that in the above works, the pure form of the fluids is considered. However, water and air in natural form contains impurities like foreign bodies and dust particles. The fluid that has dust particles mixed in it is labelled as dusty fluid. The dusty fluids are of great importance. The unrefined crude oil and petroleum, fruit juices with pulp fibers, paints with particles like glitter suspended in it are few examples of dusty fluids. In Saffman (1962) studied the gas flow containing the dust particles in it. This research derived the interest of many researchers towards the dusty fluids and their applications. Kumar (1980) assumed the geometry of the wavy wall and studied two-dimensional dusty fluid past through it. The effects of wall properties on the dusty fluid were presented by Rathod and Kulkarni (2011). The passage was considered porous as well. Hayat et al. (2014) investigated the dusty fluid under the influence of Joule and radiative heating effects along with the wall properties. Khan and Tariq (2018).assumed the Walter's B dusty fluid in a passage under the impact of wall properties. Bhatti et al. (2017) used the Jeffrey fluid with particle suspended in it to analyze the thermal radiation effects in a duct.

The ambition of this study is to analyze the dusty fluid passing through a tube. No attempt has been made to investigate the dusty fluid in a cylinder or tube that is exhibiting the peristaltic transport. Dusty second-grade fluid flowing past the asymmetric passage has been considered. This research can be useful in petroleum industry, paint industry and papermaking industry. Motion equations for dust and fluid have been modeled. DSolver has been exploited to get the solution. Results are exhibited by streamline and pressure graphs.

MATHEMATICAL FORMULATION

Axisymmetric flow of a second-grade fluid contains small spherical particles in a tube was taken. These particles are even in size. Therefore, the number density N of the solid granules are presumed to be constant. The walls of the tube are propagated with constant speed c. The cylindrical coordinate structure $(\bar{R}, \bar{Z})$ was selected.In the radial and axial directions, the velocity elements were taken as $\bar{U}$, $\bar{W}$ for fluid and $\bar{U}_s$ and $\bar{W}_s$ for dust particles.

The walls of the tube are given as:

$$\bar{R}(\bar{Z}, \bar{t}) = a + b\sin\frac{2\pi}{\lambda}(\bar{Z} - c\bar{t}), \tag{1}$$

The geometry is given in Figure 1.

For second-grade fluid, extra stress tensor is specified by $\bar{T}$.

$$\bar{T} = \mu\overline{A_1} + \alpha_1\overline{A_2} + \alpha_2\overline{A_1}^2, \tag{2}$$

$$\overline{A_1} = (grad\,\bar{V}) + (grad\,\bar{V})^t \tag{3}$$

$$\overline{A_2} = \frac{d\bar{A_1}}{dt} + \overline{A_1}(grad\,\bar{V}) + (grad\,\bar{V})^t\overline{A_1}. \tag{4}$$

In the fixed frame $(\bar{R}, \bar{Z})$, the equations expressing the movement of the fluid are [9]

$$\frac{d}{d\bar{t}}(\bar{U}, \bar{W}) = 0, \tag{5}$$

$$\rho\frac{d}{d\bar{t}}(\bar{U}) = -\frac{\partial\bar{p}}{\partial\bar{R}} + \frac{1}{R}\frac{\partial}{\partial R}(R\bar{T}_{rr}) + \frac{\partial}{\partial\bar{Z}}(\bar{T}_{rz}) + KN(\bar{U}_s - \bar{U}) \tag{6}$$

$$\rho\frac{d}{d\bar{t}}(\bar{W}) = -\frac{\partial\bar{p}}{\partial\bar{Z}} + \frac{1}{R}\frac{\partial}{\partial R}(R\bar{T}_{rz}) + \frac{\partial}{\partial\bar{Z}}(\bar{T}_{zz}) + KN(\bar{W}_s - \bar{W}) \tag{7}$$

and for solid grains [42]

$$\frac{d}{dt}(\bar{U}_s, \bar{W}_s) = 0 \tag{8}$$

$$\frac{d}{d\bar{t}}(\bar{U}) = \frac{K}{m}(\bar{U} - \bar{U}_s) \tag{9}$$

$$\frac{d}{d\bar{t}}(\bar{W}) = \frac{K}{m}(\bar{W} - \bar{W}_s), \tag{10}$$

Using the transformations mentioned below to associate the moving $(\bar{r}, \bar{z})$ and fixed frames $(\bar{R}, \bar{Z})$

$$\bar{z} = \bar{Z} - c\bar{t}, \quad \bar{r} = \bar{R}, \quad \bar{w} = \bar{W} - c, \quad \bar{u} = \bar{U}, \quad \bar{w}_s = \bar{W}_s - c, \quad \bar{u}_s = \bar{U}_s,$$

and taking into account the dimensionless quantities

$$w = \frac{\bar{w}}{c}, \qquad r = \frac{\bar{r}}{a}, \qquad z = \frac{\bar{z}}{\lambda}, \qquad p = \frac{a^2\bar{p}}{\lambda\mu c},$$
$$u_s = \frac{\bar{u}_s}{\delta c}, \qquad w_s = \frac{\bar{w}_s}{c}, \quad t = \frac{c\bar{t}}{\lambda}, \quad u = \frac{\bar{u}}{\delta c},$$
$$\delta = \frac{a}{\lambda}, \quad Re = \frac{\rho c a}{\mu}, \quad T = \frac{a\bar{T}}{\mu c}, \quad \alpha = \frac{c\bar{\alpha}}{\mu a}, \quad A = \frac{KNa^2}{\mu}, \quad B = \frac{Ka}{mc}.$$

Components of extra stress tensor are:

$$T_{rr} = 2\delta\frac{\partial u}{\partial r} + \alpha\left[\left(\frac{\partial w}{\partial r}\right)^2 + 2\delta^2 u\left(\frac{\partial^2 u}{\partial r^2}\right) + 2\delta^2 w\left(\frac{\partial^2 u}{\partial r\partial z}\right) - \delta^4\left(\frac{\partial u}{\partial z}\right)^2\right] \tag{11}$$

$$T_{rz} = \left(\delta^2\frac{\partial u}{\partial z} + \frac{\partial w}{\partial r}\right) + \alpha\left[\delta^3 u\left(\frac{\partial^2 u}{\partial r\partial z}\right) + \delta u\left(\frac{\partial^2 w}{\partial r^2}\right) + \delta^3 w\left(\frac{\partial^2 u}{\partial z^2}\right) + \delta w\left(\frac{\partial^2 w}{\partial r\partial z}\right) + \delta^3\left(\frac{\partial u}{\partial r}\right)\left(\frac{\partial u}{\partial z}\right) + \delta\left(\frac{\partial w}{\partial r}\right)\left(\frac{\partial w}{\partial z}\right) - \delta^3\left(\frac{\partial w}{\partial z}\right)\left(\frac{\partial u}{\partial z}\right) - \delta\left(\frac{\partial u}{\partial r}\right)\left(\frac{\partial w}{\partial r}\right)\right], \tag{12}$$

$$T_{zz} = 2\delta\frac{\partial w}{\partial z} + \alpha\left[\delta^4\left(\frac{\partial u}{\partial z}\right)^2 + 2\delta^2 u\left(\frac{\partial^2 w}{\partial r\partial z}\right) + 2\delta^2 w\left(\frac{\partial^2 w}{\partial z^2}\right) - \left(\frac{\partial w}{\partial r}\right)^2\right] \tag{13}$$

The streamline conversions implied are:

$$w_s = \frac{1}{r}\frac{\partial\phi}{\partial r}, \qquad w = \frac{1}{r}\frac{\partial\psi}{\partial r}, \quad u = -\frac{1}{r}\frac{\partial\psi}{\partial z}, \qquad u_s = -\frac{1}{r}\frac{\partial\phi}{\partial z}$$

The compatibility equations for fluid and dust after removing the pressure gradient are:

$$Re\delta\left[\delta^2\left(-\frac{2}{r}\frac{\partial^2\psi}{\partial z^2}\frac{\partial\psi}{\partial z} - \frac{\partial^3\psi}{\partial z^3}\frac{1}{r}\frac{\partial\psi}{\partial r} + \frac{\partial\psi}{\partial z}\frac{1}{r}\right) - \left(\frac{\partial\psi}{\partial z}\frac{3}{r^2}\frac{\partial^2\psi}{\partial r^2} + \frac{\partial^3\psi}{\partial r^2\partial z}\frac{1}{r}\frac{\partial\psi}{\partial r} - \frac{\partial\psi}{\partial r}\frac{3}{r^3}\frac{\partial\psi}{\partial z} - \frac{\partial\psi}{\partial r}\frac{1}{r^2}\frac{\partial^2\psi}{\partial r\partial z} - \frac{1}{r}\frac{\partial^3\psi}{\partial r^3}\frac{\partial\psi}{\partial z}\right)\right] = \delta\frac{\partial^2}{\partial r\partial z}(rT_{rr}) - r\frac{\partial}{\partial r}\left(\frac{1}{r}\frac{\partial}{\partial r}(rT_{rz})\right) + r\delta^2\left(\frac{\partial^2 T_{rz}}{\partial z^2}\right) - r\delta\left(\frac{\partial^2 T_{zz}}{\partial z\partial r}\right) + A(\nabla_1^2\phi - \nabla_1^2\psi), \tag{14}$$
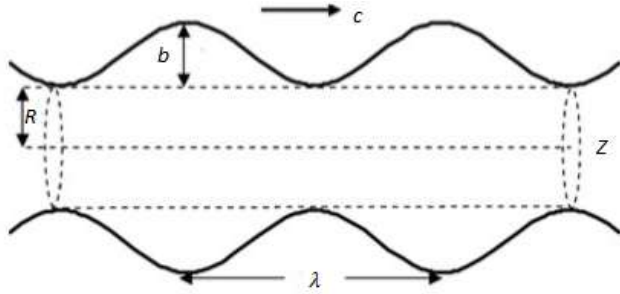
Figure 1. Geometry of the tube.

$$\delta\left[\delta^2\left(\frac{1}{r}\frac{\partial\phi}{\partial z}-\frac{\partial^3\phi}{\partial z^3}\frac{1}{r}\frac{\partial\phi}{\partial r}-\frac{\partial\phi}{\partial z}\frac{\partial^2\phi}{\partial z^2}\frac{2}{r}\right)-\left(\frac{\partial\phi}{\partial z}\frac{3}{r^2}\frac{\partial^2\phi}{\partial r^2}-\frac{\partial\phi}{\partial r}\frac{1}{r^2}\frac{\partial^2\phi}{\partial r\partial z}-\frac{\partial\phi}{\partial z}\frac{3}{r^3}\frac{\partial\phi}{\partial r}-\frac{\partial^3\phi}{\partial r^3}\frac{1}{r}\frac{\partial\phi}{\partial z}+\frac{\partial^3\phi}{\partial r^2\partial z}\frac{\partial\phi}{\partial r}\frac{1}{r}\right)\right]=$$
$$B(\nabla_1^2\phi-\nabla_1^2\psi).$$

(15)

where $\nabla_1^2=\left(\delta^2\frac{\partial^2}{\partial z^2}+\frac{\partial^2}{\partial r^2}-\frac{1}{r}\frac{\partial}{\partial r}\right)$.

Walls geometry in dimensionless configuration is:

$h=1+\varphi\,sinz$
(16)

The non-dimension boundary conditions are:

$\psi=0,\quad\phi=0,\quad\frac{\partial}{\partial r}\left(\frac{1}{r}\frac{\partial\psi}{\partial r}\right)=0\quad at\quad r=0$ (17)

$\psi=F,\quad\phi=F_s,\quad\frac{1}{r}\frac{\partial\psi}{\partial r}=-1\quad at\quad r=h$ (18)

The dimensionless time flow of the fluid and the solid granules are given as:

$Q=F+0.5\left(1+\frac{\varphi^2}{2}\right)$ (19)

$Q_s=F_s+0.5\left(1+\frac{\varphi^2}{2}\right)$ (20)

Where

$F=\int_0^h\frac{\partial\psi}{\partial r}dr=\psi(h)-\psi(0)$ (21)

$F_s=\int_0^h\frac{\partial\phi}{\partial r}dr=\phi(h)-\phi(0)$ (22)

The expression for the pressure rise is:

$\Delta P=\int_0^{2\pi}\frac{dp}{dr}dr$ (23)

Solution methodology

The equations obtained for the dust and the fluid particles are non-linear in nature. To obtain the solution, perturbation technique has been adopted.

$\psi=\psi_0+\delta\psi_1+\delta^2\psi_2+O(\delta^3)$ (24a)

$F=F_0+\delta F_1+\delta^2F_2+O(\delta^3)$

(24b)

$\phi=\phi_0+\delta\phi_1+\delta^2\phi_2+O(\delta^3)$ (24c)

$F_s=F_{s0}+\delta F_{s1}+\delta^2F_{s2}+O(\delta^3)$ (24d)

$p=p_0+\delta p_1+\delta^2p_2+O(\delta^3)$ (24e)

Zeroth-order system

$\left(\frac{\partial^2}{\partial r^2}-\frac{1}{r}\frac{\partial}{\partial r}\right)\left[(rT_{0rz}-A(\phi_0-\psi_0))\right]=0$ (25)

$\left(\frac{\partial^2}{\partial r^2}-\frac{1}{r}\frac{\partial}{\partial r}\right)\left(B(\phi_0-\psi_0)\right)=0$ (26)

$\frac{dp_0}{dz}=\frac{1}{r}\left(T_{0rz}+r\frac{\partial}{\partial r}(T_{0rz})\right)+\frac{A}{r}\left(\frac{\partial}{\partial r}(\psi_0-\phi_0)\right)$ (27)

Where
$T_{0rz}=-\frac{1}{r}\left(\frac{1}{r}\frac{\partial\psi_0}{\partial r}+\frac{\partial^2\psi_0}{\partial r^2}\right)$ (28)

With

$\psi_0=0,\quad\phi_0=0,\quad\frac{\partial}{\partial r}\left(\frac{1}{r}\frac{\partial\psi_0}{\partial r}\right)=0\ at\ r=0$ (29)

$\psi_0=F_0,\quad\phi_0=F_{s0},\quad\frac{1}{r}\frac{\partial\psi_0}{\partial r}=-1\ at\ r=h$ (30)

Solution of zeroth-order

$\psi_0=\frac{1}{2}r^2A_1+\frac{1}{4}r^4A_2,$

$\phi_0=\frac{A_2r^4}{4}+\frac{1}{2}r^2A_3,$

$A_1=1+\frac{4F_0}{h^2},A_2=\frac{-2(2F_0+h^2)}{h^4},A_3=-\frac{A_2h^2}{2}+\frac{2F_{s0}}{h^2}.$

This solution is same as obtained by Siddiqui and Schwarz (1994).

First order system

$$Re\frac{1}{r}\left(-\frac{\partial\psi_0}{\partial r}\frac{\partial^3\psi_0}{\partial r^2\partial z}+\frac{\partial\psi_0}{\partial z}\frac{3}{r^2}\frac{\partial\psi_0}{\partial r}+\frac{\partial^3\psi_0}{\partial r^3}\frac{\partial\psi_0}{\partial z}-\frac{\partial\psi_0}{\partial z}\frac{3}{r}\frac{\partial^2\psi_0}{\partial r^2}+\frac{\partial^2\psi_0}{\partial z\partial r}\frac{\partial\psi_0}{\partial r}\frac{1}{r}\right)$$
$$=A\left(\left(-\frac{1}{r}\frac{\partial}{\partial r}+\frac{\partial^2}{\partial r^2}\right)(\phi_1-\psi_1)-r\frac{\partial}{\partial r}\left(\frac{1}{r}\frac{\partial}{\partial r}(rT_{1rz})\right)+\frac{\partial^2}{\partial z\partial r}(rT_{0rr})\left(r\frac{\partial^2T_{0zz}}{\partial z\partial r}\right),$$

(31)

$$\left(\frac{1}{r}\left(-\frac{\partial\phi_0}{\partial z}\frac{3}{r^2}\frac{\partial^2\phi_0}{\partial r^2}+\frac{\partial\phi_0}{\partial z}\frac{3}{r^3}\frac{\partial\phi_0}{\partial r}+\frac{\partial^2\phi_0}{\partial r\partial z}\frac{1}{r^2}\frac{\partial\phi_0}{\partial r}-\frac{1}{r}\frac{\partial^3\phi_0}{\partial z\partial r^2}\frac{\partial\phi_0}{\partial r}+\frac{\partial\phi_0}{\partial z}\frac{\partial^3\phi_0}{\partial r^3}\frac{1}{r}\right)\right)=B\left(\left(\frac{\partial^2}{\partial r^2}-\frac{1}{r}\frac{\partial}{\partial r}\right)(\phi_1-\psi_1)\right),$$

(32)

$\frac{dp_1}{dz}=\left(\frac{\partial T_{0zz}}{\partial z}\right)+\frac{1}{r}\left(\frac{\partial}{\partial r}(rT_{1rz})\right)+\frac{A}{r}\left(\frac{\partial\psi_1}{\partial r}-\frac{\partial\phi_1}{\partial r}\right)-Re\left(\frac{\partial\psi_0}{\partial z}\frac{1}{r^3}\frac{\partial\psi_0}{\partial r}-\frac{\partial\psi_0}{\partial z}\frac{\partial^2\psi_0}{\partial r^2}\frac{1}{r^2}+\frac{\partial\psi_0}{\partial r}\frac{\partial^2\psi_0}{\partial r\partial z}\frac{1}{r^2}\right)$ (33)

Where

$T_{1rz}=\frac{1}{r}\left(-\frac{\partial^2\psi_1}{\partial r^2}+\frac{\partial\psi_1}{\partial r}\frac{1}{r}\right)+\alpha\left[\frac{2}{r^2}\frac{\partial^2\psi_0}{\partial r\partial z}\frac{\partial^2\psi_0}{\partial r^2}+\frac{1}{r^2}\frac{\partial\psi_0}{\partial r}\frac{\partial^3\psi_0}{\partial r^2\partial z}-\frac{1}{r^2}\frac{\partial\psi_0}{\partial z}\frac{\partial^3\psi_0}{\partial r^3}-\frac{\partial\psi_0}{\partial z}\frac{\partial\psi_0}{\partial r}\frac{1}{r^4}+\frac{1}{r^3}\frac{\partial\psi_0}{\partial z}\frac{\partial^2\psi_0}{\partial r^2}-\frac{\partial\psi_0}{\partial r}\frac{\partial^2\psi_0}{\partial r\partial z}\frac{3}{r^3}\right],$ (34)

$$T_{0rr} = \alpha \left[\frac{\partial}{\partial r} \left(-\frac{1}{r} \frac{\partial \psi_0}{\partial r} \right) \right]^2 \tag{35}$$

$$T_{0zz} = -\alpha \left[\frac{\partial}{\partial r} \left(-\frac{1}{r} \frac{\partial \psi_0}{\partial r} \right) \right]^2 \tag{36}$$

With

$$\psi_1 = 0, \quad \phi_1 = 0, \quad \frac{\partial}{\partial r} \left(\frac{1}{r} \frac{\partial \psi_1}{\partial r} \right) = 0 \ at \ \ r = 0 \tag{37}$$

$$\psi_1 = F_1, \quad \phi_1 = F_{s1}, \quad \frac{1}{r} \frac{\partial \psi_1}{\partial r} = 0 \ at \ r = h$$

Solution of first order

$$\psi_1 = -\frac{1}{96} AA_2' A_3 r^6 - \frac{1}{576} AA_2' A_2 r^8 + \frac{1}{96} A_1 A_2' r^6 Re + \frac{1}{576} A_2' A_2 r^8 Re + \frac{1}{2} r^2 B_1 + \frac{1}{4} r^4 B_2, \tag{38}$$

$$\phi_1$$
$$= \frac{(-A_2' A_3 + BB_2) r^4}{4B}$$
$$+ \frac{\left(-A_2' A_2 + 12B \left(-\frac{1}{96} AA_2' A_3 \right) + 12B \left(\frac{1}{96} A_1 A_2' Re \right) \right) r^6}{12B}$$
$$+ \left(-\frac{1}{576} AA_2' A_2 + \frac{1}{576} A_2' A_2 Re \right) r^8 + \frac{1}{2} r^2 B_3,$$

$$B_1 = \frac{576 F_1 + A_2' h^6 (-3AA_3 - AA_2 h^2 + 3A_1 Re + A_2 h^2 Re)}{144 h^2},$$

$$B_2 = \frac{-192 F_1 + A_2' h^6 (4AA_3 + AA_2 h^2 - 4A_1 Re - A_2 h^2 Re)}{48 h^4},$$

$$B_3$$
$$= \frac{1}{6Bh^2} \left(A_2'(3A_3 h^4 + A_2 h^6) \right.$$
$$\left. - 3B \left(B_1 h^4 + 4 \left(\begin{array}{c} \left(\frac{1}{96} AA_2' A_3 \right) h^6 + \left(\frac{1}{96} Re A_2' A_3 \right) h^6 \\ - \left(\frac{1}{576} AA_2' A_2 \right) h^8 + \left(\frac{1}{576} AA_2' A_2 \right) h^8 - F_{s1} \end{array} \right) \right) \right).$$

In the absence of solid particles, this solution is same as obtained by Siddiqui and Schwarz (1994).

Second order system

$$Re \frac{1}{r} \left(-\frac{\partial \psi_1}{\partial z} \frac{\partial^2 \psi_1}{\partial r^2} \frac{3}{r} + \frac{\partial^3 \psi_1}{\partial r^3} \frac{\partial \psi_1}{\partial z} + \frac{\partial \psi_1}{\partial z} \frac{3}{r^2} \frac{\partial \psi_1}{\partial r} - \frac{\partial^3 \psi_1}{\partial z \partial r^2} \frac{\partial \psi_1}{\partial r} + \frac{\partial \psi_1}{\partial r} \frac{\partial^2 \psi_1}{\partial r \partial z} \frac{1}{r} \right) =$$
$$\frac{\partial^2}{\partial z \partial r} (r T_{1rr}) + r \left(\frac{\partial^2 T_{0rz}}{\partial z^2} \right) - r \left(\frac{\partial^2 T_{1zz}}{\partial r \partial z} \right) + A \left(\left(\frac{\partial^2 z}{\partial r^2} \right) (\phi_0 - \psi_0) + \right.$$
$$\left(\frac{\partial^2}{\partial r^2} - \frac{1}{r} \frac{\partial}{\partial r} \right) (\phi_2 - \psi_2) \right) -$$
$$r \frac{\partial}{\partial r} \left(\frac{1}{r} \frac{\partial}{\partial r} (r T_{2rz}) \right), \tag{39}$$

$$\left(\frac{1}{r} \left(-\frac{\partial^2 \phi_1}{\partial r^2} \frac{\partial \phi_1}{\partial z} \frac{3}{r} - \frac{\partial \phi_1}{\partial r} \frac{\partial^3 \phi_1}{\partial r^2 \partial z} + \frac{\partial \phi_1}{\partial z} \frac{\partial^3 \phi_1}{\partial r^3} + \frac{\partial \phi_1}{\partial r} \frac{\partial^2 \phi_1}{\partial z \partial r} \frac{1}{r} + \frac{\partial \phi_1}{\partial z} \frac{\partial \phi_1}{\partial r} \frac{3}{r^2} \right) \right)$$
$$= B \left(\left(\frac{\partial^2 z}{\partial r^2} \right) (\phi_0 - \psi_0) + \left(\frac{\partial^2}{\partial r^2} - \frac{1}{r} \frac{\partial}{\partial r} \right) (\phi_2 - \psi_2) \right), \qquad \frac{dp_2}{dz}$$
$$= \left(\frac{\partial T_{1zz}}{\partial z} \right) + \left(\frac{1}{r} \frac{\partial}{\partial r} (r T_{1rz}) \right) + \frac{A}{r} \left(\frac{\partial \psi_2}{\partial r} - \frac{\partial \phi_2}{\partial r} \right) - Re \left(\frac{\partial \psi_1}{\partial z} \frac{1}{r^3} \frac{\partial \psi_1}{\partial r} - \frac{1}{r^2} \frac{\partial^2 \psi_1}{\partial r^2} \frac{\partial \psi_1}{\partial z} + \frac{1}{r^2} \frac{\partial \psi_1}{\partial r} \frac{\partial^2 \psi_1}{\partial r \partial z} \right) \tag{40}$$

Where,

$$T_{2rz} = \left(-\frac{\partial^2 \psi_1}{\partial r^2} \frac{1}{r} + \frac{1}{r^2} \frac{\partial \psi_1}{\partial r} + \frac{1}{r} \frac{\partial^2 \psi_0}{\partial z^2} \right) + \alpha \left[\frac{2}{r^2} \frac{\partial^2 \psi_1}{\partial r^2} \frac{\partial^2 \psi_1}{\partial r \partial z} - \frac{1}{r^4} \frac{\partial \psi_1}{\partial z} \frac{\partial \psi_1}{\partial r} + \right.$$
$$\frac{\partial \psi_1}{\partial z} \frac{1}{r^3} \frac{\partial^2 \psi_1}{\partial r^2} - \frac{3}{r^3} \frac{\partial \psi_1}{\partial r} \frac{\partial^2 \psi_1}{\partial r \partial z} - \frac{1}{r^2} \frac{\partial \psi_1}{\partial z} \frac{\partial^3 \psi_1}{\partial r^3} +$$
$$\left. \frac{\partial \psi_1}{\partial r} \frac{1}{r^2} \frac{\partial^3 \psi_1}{\partial r^2 \partial z} \right], \tag{41}$$

$$T_{1rr} = \left(-\frac{\partial \psi_0}{\partial z} \frac{2}{r^2} + \frac{2}{r} \frac{\partial^2 \psi_0}{\partial z \partial r} \right) - \alpha \left[\frac{\partial}{\partial r} \left(-\frac{1}{r} \frac{\partial \psi_1}{\partial r} \right) \right]^2 \tag{43}$$

$$T_{1zz} = \left(-\frac{\partial^2 \psi_0}{\partial z \partial r} \frac{2}{r} \right) + \alpha \left[\frac{\partial}{\partial r} \left(-\frac{1}{r} \frac{\partial \psi_1}{\partial r} \right) \right]^2 \tag{44}$$

With

$$\psi_2 = 0, \ \phi_2 = 0, \quad \frac{\partial}{\partial r} \left(\frac{1}{r} \frac{\partial \psi_2}{\partial r} \right) = 0 \ at \ \ r = 0 \psi_2 = F_2, \quad \phi_2 = F_{s2}, \ \frac{1}{r} \frac{\partial \psi_2}{\partial r} \tag{42}$$

$$= 0 \ at \ r = h.$$

These systems of equations are solved by using DSolver methodology in Mathematica software.

RESULTS AND DISCUSSION

This section is dedicated to discuss the impact of diverse parameters on the velocity, streamline, pressure rise. Velocity of the fluid under the influence of Reynolds number (Re), (α), that is, the second-grade attribute and (δ) the wave number is presented in Figures 2 to 4. The graphical demonstration of the pressure gradient is shown in Figures 5 to 7. Figures 8 to 10 are plotted to examine the pressure rise. Impact of parameters on shear stress is presented in Figures 11 to 13. Streamline graphs hold an important role while studying the flow of the fluids. The pattern of the flow of the fluid is presented through the contour graphs. Figures 14 to 16 show the streamline patterns of fluid under the impact of different attributes. The consequences of these parameters on the velocity of the solid grains are illustrated in Figures 17 to 19. As the fluid contains the solid grains in it so the contour graphs for the solid grains are included as well. The contour graphs for different parameters for the solid grains are exemplified in Figures 20 to 22.

As shown in Figure 2, with the increase in wave number, the fluid flows more smoothly and efficiently in the desired direction. With the rise in the Reynolds number (Re), we see an increasing manner in the velocity in the center of the tube. As increase in Re reduces the friction force thus causing rise in the fluid velocity. Growth in α, enhances the velocity of the fluid as demonstrated in Figure 4. The pressure gradient $\frac{dp}{dz}$ versus z is given in Figures 5 to 7 for the impact of Re, α and δ respectively. It is noted that small pressure gradient has been occurred in $z \in [1,3]$. It means that the flow can smoothly go through without imposition of large pressure gradient and large pressure gradient occurs for $z \in [3,7]$. It means greater pressure gradient is required to
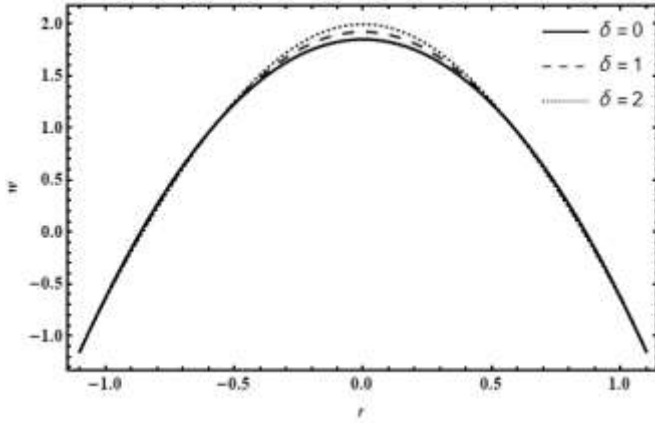
Figure 2. Velocity presentation of fluid for $\varphi = 0.15$, $Q = 0.75$, $\alpha = 1.5$, $A = 1$, $B = 1$, $Re = 5$ and $Q_s = 0.5$.
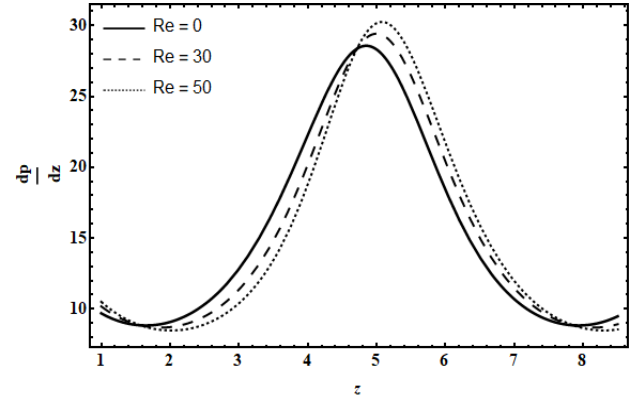

Figure 5. The pressure gradient dp/dz versus z with $Q = 0.9$, $\alpha = 1.5$, $A = 2$, $B = 2$, $\delta = 0.02$, $Q_s = 0.8$ and $\varphi = 0.2$,.
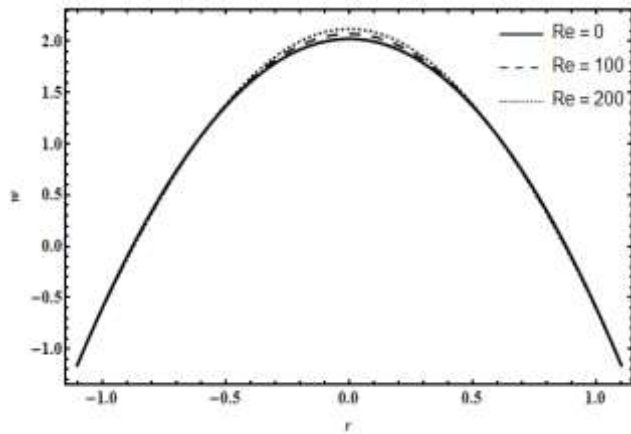

Figure 3. Velocity presentation of fluid for $\varphi = 0.15$, $Q = 0.75$, $\alpha = 1.5$, $A = 1$, $B = 1$, $\delta = 0.5$ and $Q_s = 0.5$.
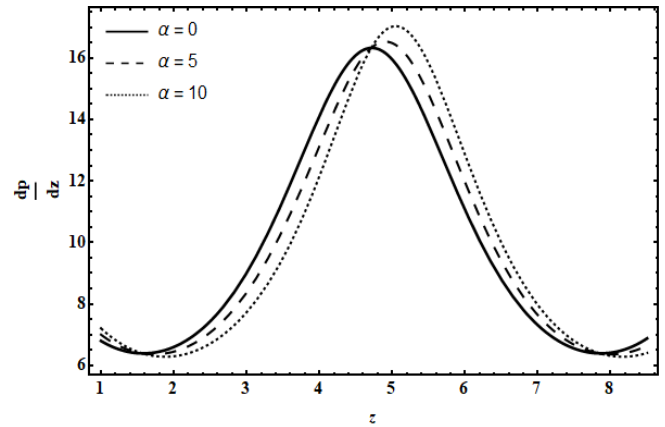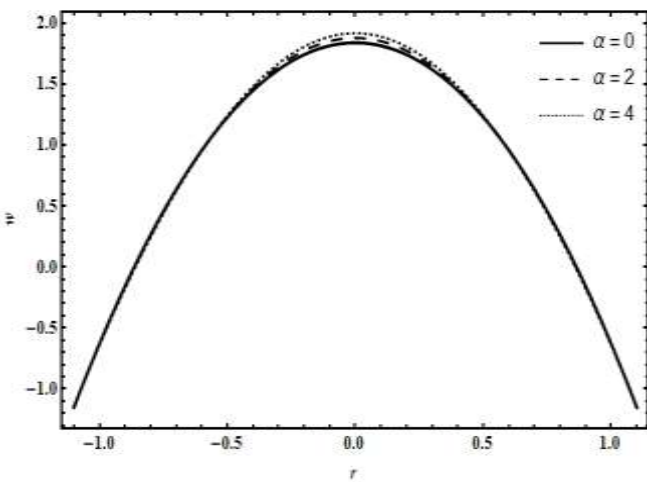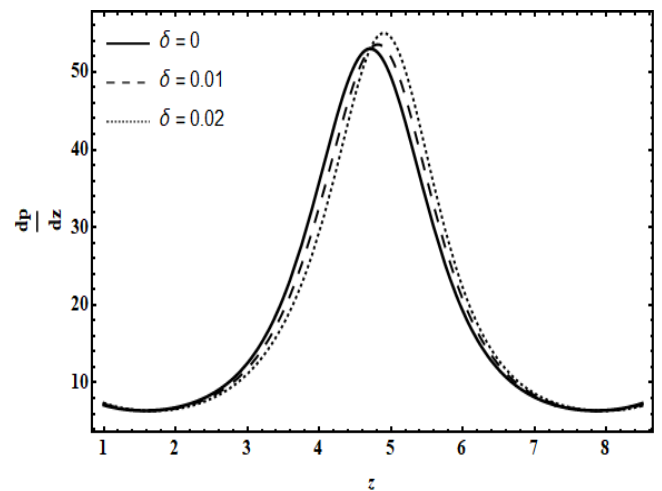

Figure 6. The pressure gradient dp/dz versus z with $Q = 0.6$, $Re = 5$ $A = 1$, $B = 2$, $\delta = 0.02$, $Q_s = 0.5$ and $\varphi = 0.15$.

Figure 4. Velocity presentation of fluid for $\varphi = 0.15$, $Q = 0.75$, $Re = 5$, $A = 1$, $B = 1$, $\delta = 0.5$ and $Q_s = 0.5$.

Figure 7. The pressure gradient dp/dz versus z with $Q = 0.9$, $Re = 5$ $A = 2$, $B = 2$, $\alpha = 1.5$, $Q_s = 0.8$ and $\varphi = 0.35$.
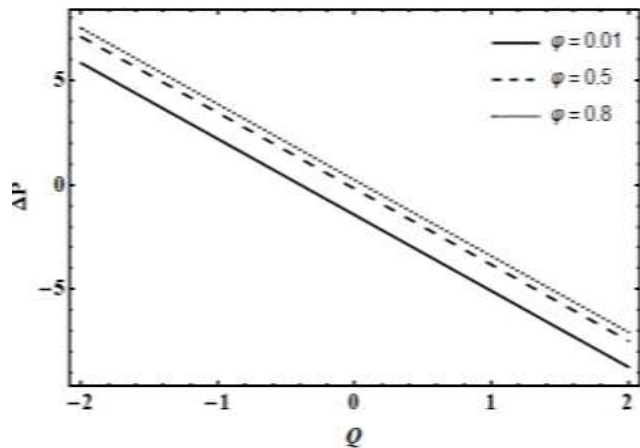
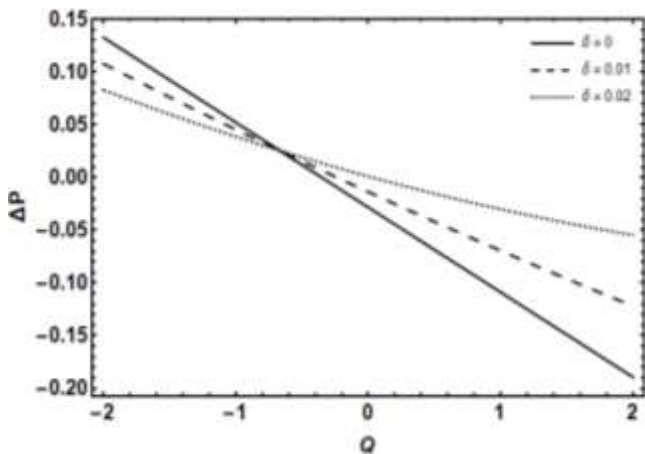**Figure 8.** The pressure rise ΔP versus Q with $\delta = 0.01, Re = 5$ $A = 2, B = 2$ and $\alpha = 1.5$.

Figure 9. The pressure rise ΔP versus Q with $\varphi = 0.15, Re = 5$ $A = 1, B = 2, \alpha = 1.5$.
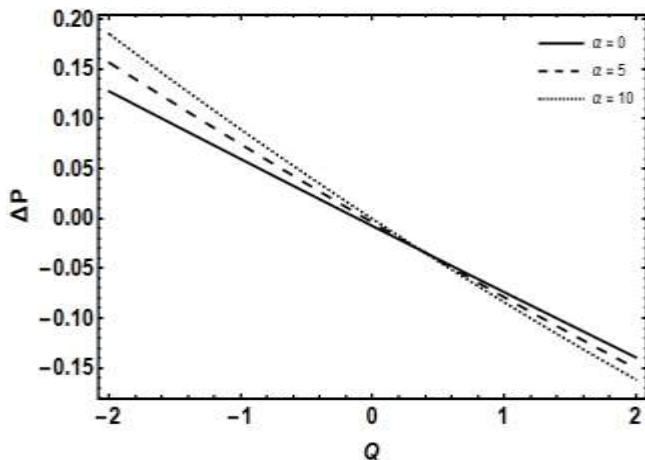

Figure 10. The pressure rise ΔP versus Q with $\varphi = 0.15, Re = 2.5, A = 1, B = 2$ and $\delta = 0.01$.
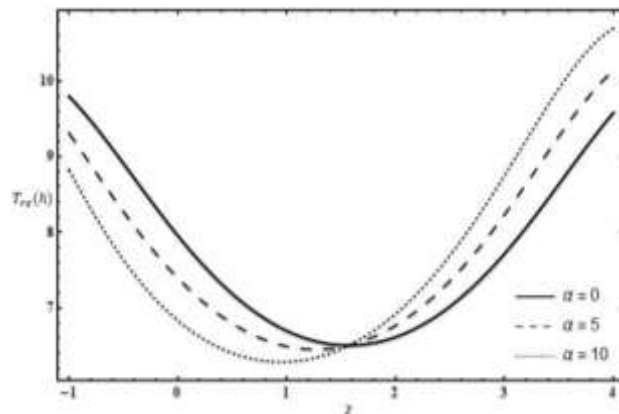
Figure 11. The shear stress at wall with $\varphi = 0.15, Re = 5, A = 1, B = 2, \delta = 0.01, Q = 0.8$ and $Q_s = 0.7$.
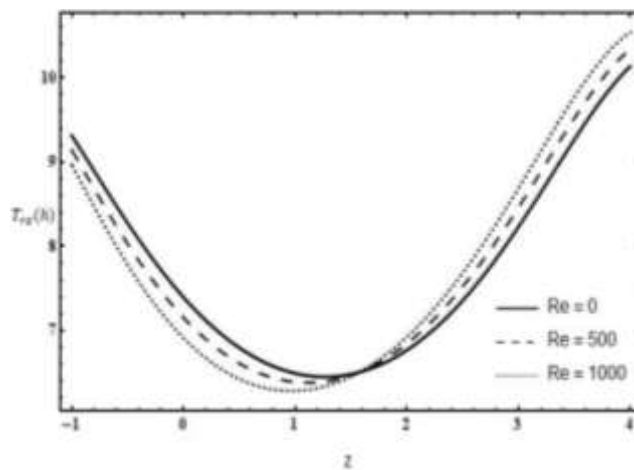

Figure 12. The shear stress at wall with $\varphi = 0.15, \alpha = 5, A = 1, B = 2, \delta = 0.01, Q = 0.8$ and $Q_s = 0.7$.
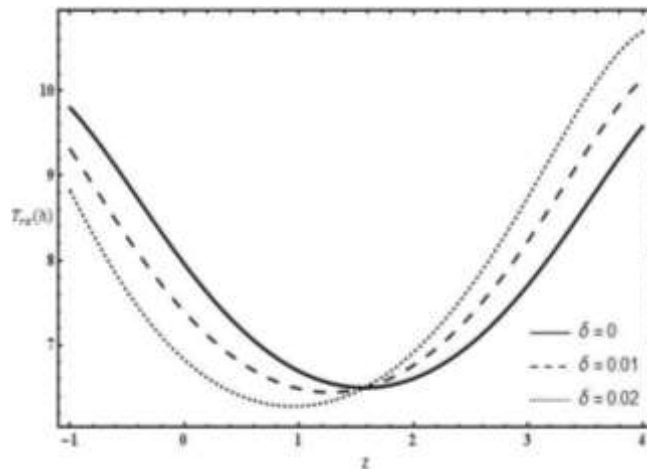

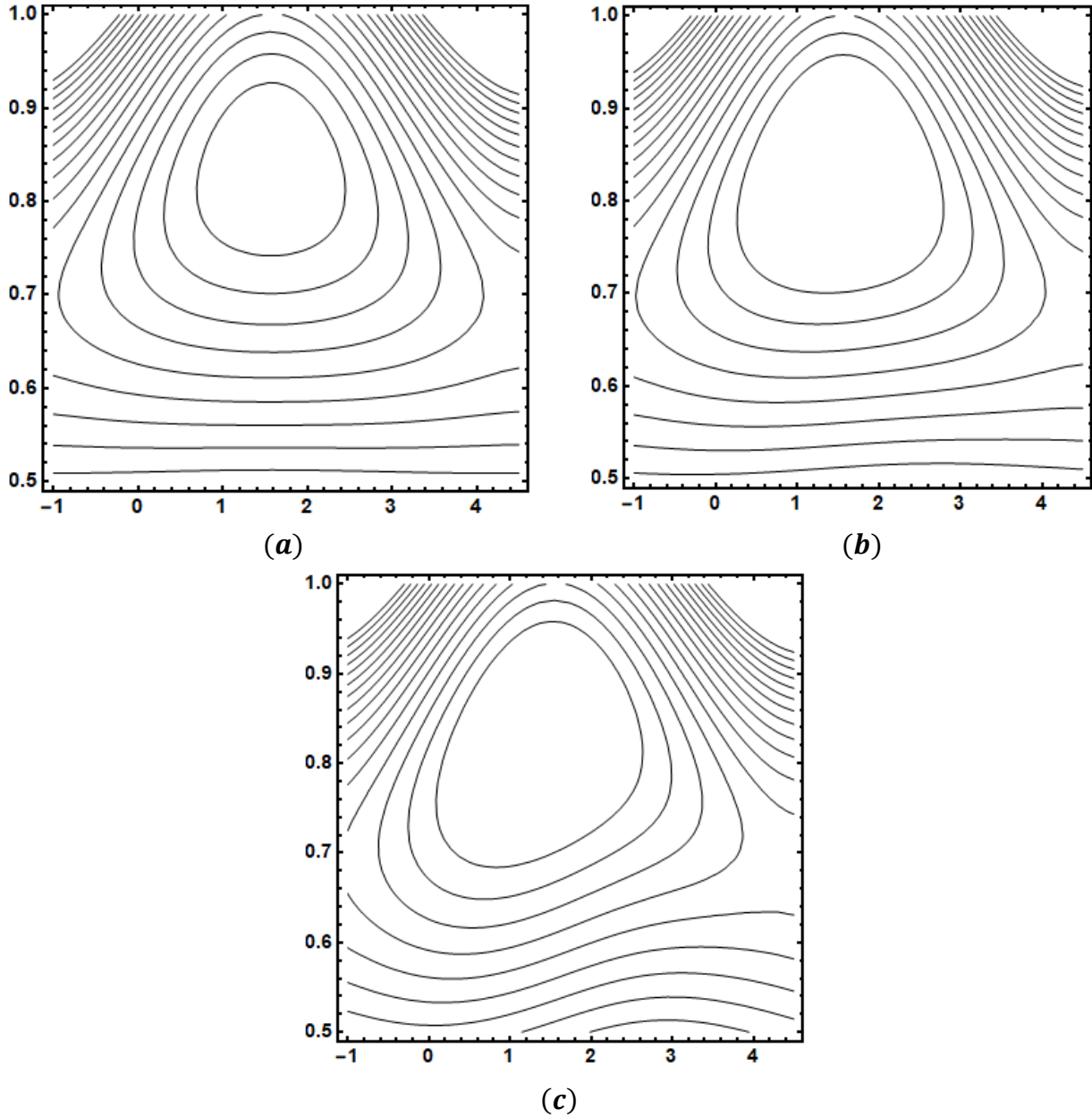**Figure 13.** The shear stress at wall with $\varphi = 0.15, Re = 5, A = 1, B = 2, \alpha = 2, Q = 0.8$ and $Q_s = 0.7$.

Figure 14. Streamline presentation of fluid for $(a)\,\delta = 0$ $(b)\,\delta = 0.1$ $(c)\,\delta = 0.5$ with $\varphi = 0.12$, $\alpha = 5, A = 1, B = 2, Re = 50, Q = 0.6 \; and \; Q_s = 0.9$.

attain same flux to pass it. Figures 8 show the influence of φ on pressure rise. As the amplitude is increased, it is concluded that more pressure is needed to pump the fluid throughout the region. The pumping rate falls in the retrograde region $(\Delta P > 0)$ as the wave number increases. While a reverse situation can be observed in co-pumping region $(\Delta P < 0)$. The retrograde region broadens with the increase in α. Pumping rate grows with the increase in second grade parameter. Impression of different parameters on wall shear stress T_{rz} at $r = h$, are demonstrated in Figures 11 to 13. With the increase in

the parameters, it can be seen that the walls of the tube are exhibiting to and fro movement thus the peristaltic motion of the wall can be seen clearly.

Figure 14 shows that as the values of the wave number (δ) is raised, the bolus in the channel get enhanced. As wave number is increased, the movement of bolus can be seen stretching towards the upward direction. The impact of Reynolds number (Re) on the streamline pattern is shown in Figure 15. As the Reynolds number is increased, viscous force weakens thus it was observed that the motion of the fluid gets smoother and bolus
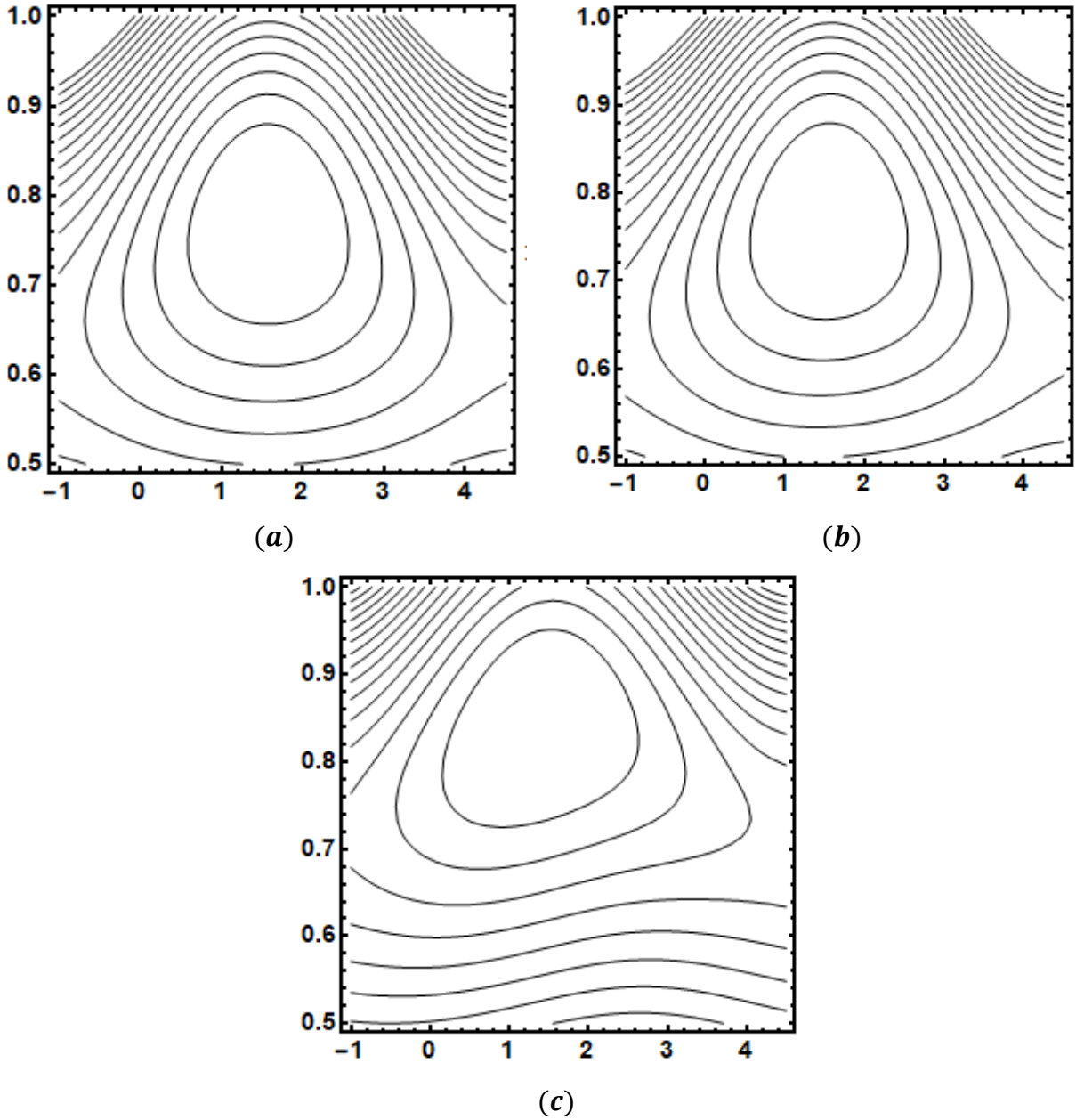
Figure 15. Streamline presentation of fluid for $(a)\ Re = 0\ (b)\ Re = 100\ (c)\ Re = 200$ with $\varphi = 0.1,\ \alpha = 1.5, A = 1, B = 2, \delta = 0.06, Q = 0.65$ and $Q_s = 0.6$.

expands and move towards upward direction. The streamline patterns for the amplitude ratio (φ) is illustrated in Figure 16. For $\varphi = 0$, no bolus is formed as shown in Figure 16(a). As the values of φ are increased, a clear change in the formation and volume of the bolus was observed. The motion of the fluid particles is towards the direction of the amplitude of the tube.

The impact of parameters like (δ), Re and (α) on the velocity of the solid grains is given in Figures 17 to 19. Increase in the velocity for (δ) and for Re, growth in the velocity of the solid grains was observed. Increase in

Reynolds number refers that viscous forces are weakening thus particles may flow more smoothly but for the second-grade parameter (α), we observe no change in the velocity of the solid grains at least to $O(\delta^2)$ was observed Figure 20 shows the impact of (δ) on the contour patterns of the solid grains. As the wave number grows, an expansion in the volume of the bolus was seen. This indicates that the movement of particles is expanding. The enlargement in the Reynolds number (Re) enhances the bolus as illustrated in Figure 21. With lower viscous force, the bolus formed shows that the
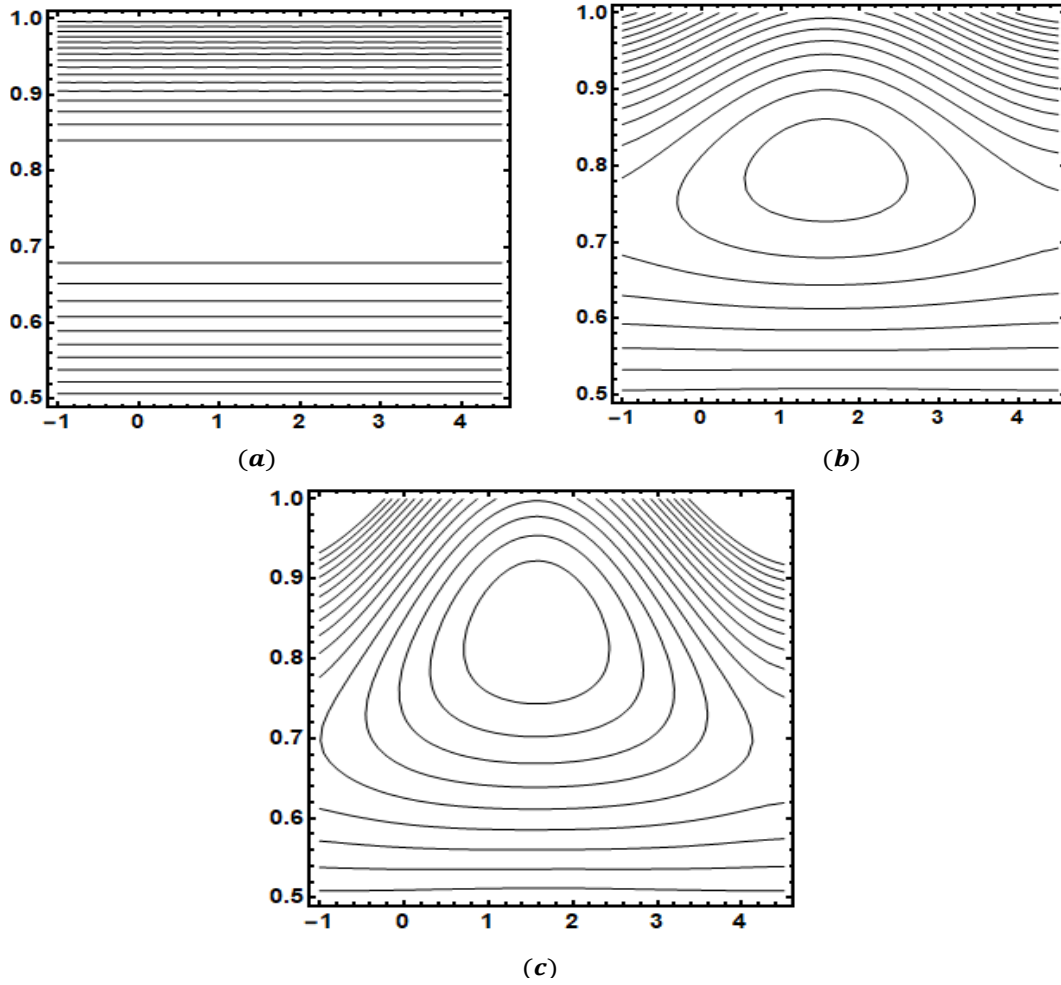
Figure 16. Streamline presentation of fluid for $(a)\ \varphi = 0$ $(b)\ \varphi = 0.05$ $(c)\ \varphi = 0.12$ with $Q = 0.6,\ \alpha = 1.5, A = 1, B = 2, \delta = 0.06\ and\ Re = 5, Q_s = 0.9$.

Figure 17. Velocity presentation of solid grains for $\varphi = 0.15,\ Q = 0.9,\ Re = 5, A = 1, B = 1,\ \alpha = 1.5\ and\ Q_s = 0.7$.

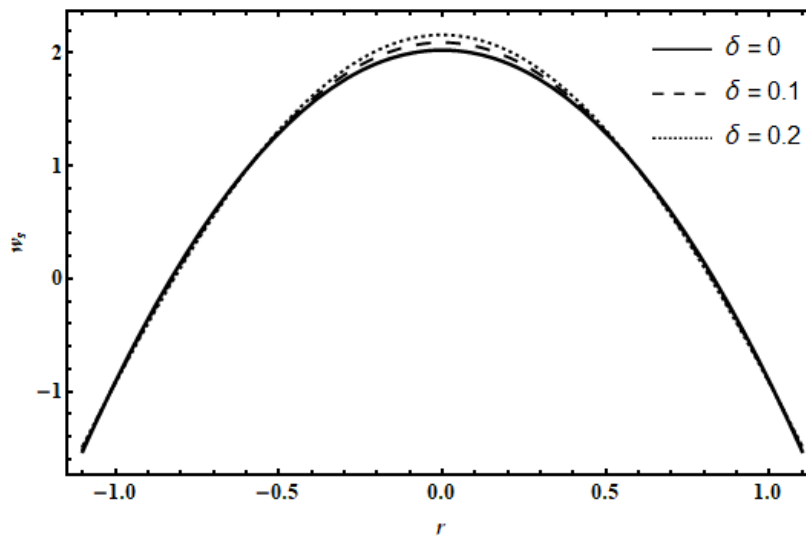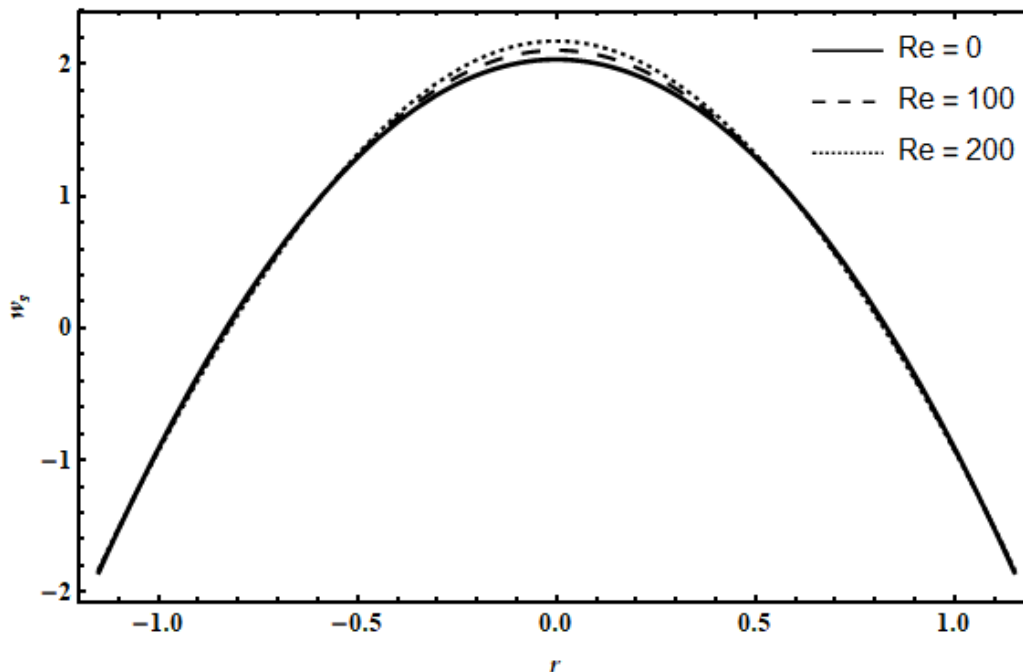**Figure 18.** Velocity presentation of solid grains for $\varphi = 0.15$, $Q = 0.9$, $\delta = 0.5$, $A = 1$, $B = 1$, $\alpha = 1.5$ and $Q_s = 0.7$.
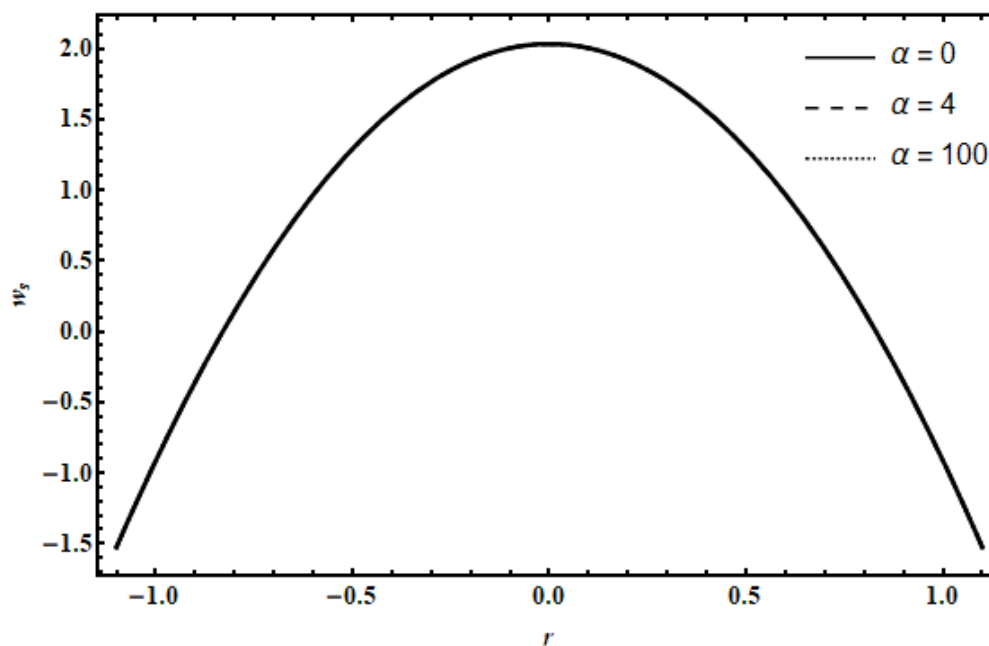

Figure 19. Velocity presentation of solid grains for $\varphi = 0.15$, $Q = 0.9$, $\delta = 0.5$, $A = 1$, $B = 1$, $Re = 10$ and $Q_s = 0.7$.

movement of particles gets smoother. With the rise in the amplitude of the wave, it was observed that the bolus is stretched upward as illustrated in Figure 22. With the increase in amplitude, the flow of the particles also moves up along the upward direction. Figure 23 shows a comparison between the velocity profile obtained by perturbation technique and numerical technique. The velocity of the fluid seems to be following same pattern
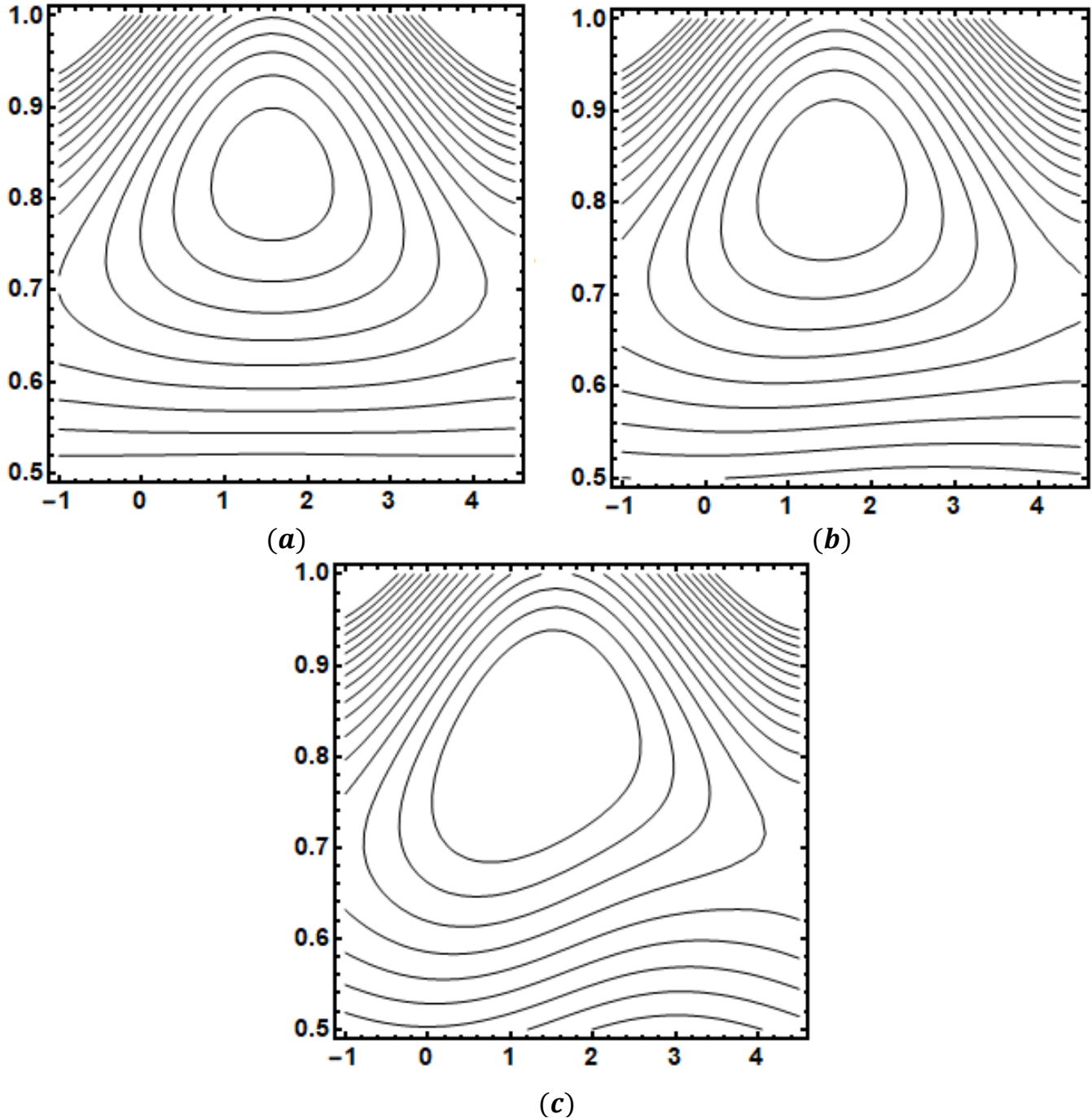
Figure 20. Streamline presentation of solid grains for (a) $\delta = 0$ (b) $\delta = 0.1$ (c) $\delta = 0.5$ with $\varphi = 0.1, \alpha = 5, A = 1, B = 2, Re = 50, Q = 0.6$ and $Q_s = 0.6.$

and ranges through both techniques.

Conclusions

In this article, the second-grade fluid containing fine dust grains in a tube was studied. Perturbation technique up to $O(\delta^2)$ has been imposed to get the solutions. The results are shown through graphs. Following results are worth mentioning:

1. The bolus expands for solid grains and fluid as the wave number enhances.
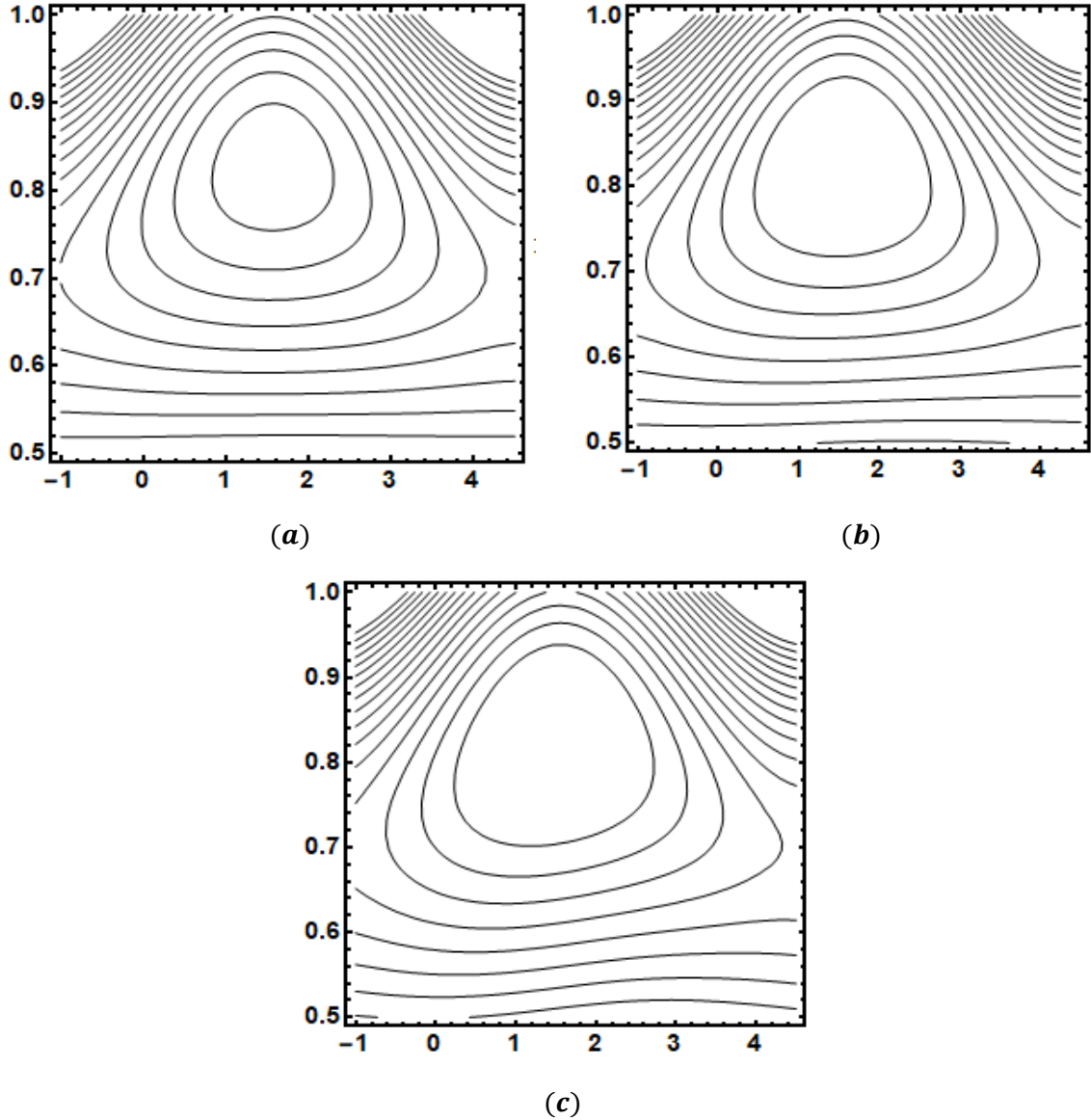2. The trapped bolus expands for dust grains and the

Figure 21. Streamline presentation of solid grains for $(a)\ Re = 0$ $(b)\ Re = 50$ $(c)\ Re = 100$ with $\varphi = 0.1, \alpha = 1.5, A = 1, B = 2, \delta = 0.05, Q = 0.6\ and\ Q_s = 0.6$.

fluid as Reynolds number *(Re)* is increased.

3. The bolus is stretched to the upward direction of the channel as the amplitude ratio is increased.

4. Growth in the velocity of the solid grains and the fluid for the parameter δ and Re.

5. In retrograde region, pumping rate increases with the increase in α and it decreases for increased values of δ.

NOMENCLATURE

a, Tube radius; **b,** wave amplitude**; λ,** wave length; **c,** wave speed; μ, shear viscosity coefficient; **N,** number density of solid particles; $\bar{t}, t$, time in laboratory and wave frame; $\bar{p}, p$, pressure in laboratory and wave frame; $\bar{A}_1, \bar{A}_2$, Rivlin-Ericksen tensor; $\bar{R}(\bar{Z}, \bar{t})$, dimensional form of walls in laboratory frame; $(\bar{U}, \bar{W}), (\bar{U}_s, \bar{W}_s)$, velocity of fluid and solid particles in dimensional form in laboratory frame; **K,** Stokes resistance coefficient; $\frac{m}{K}$, relaxation time of solid granules; $\bar{T}, T$, Extra stress tensor in laboratory and wave frame; $(u, w), (u_s, w_s)$, velocity of fluid and solid particles in dimensionless form in wave frame; δ, wave number; **Re,** Reynolds number; $\bar{\alpha}, \alpha$, second grade parameter in laboratory and wave frame; $A = \frac{KNa^2}{\mu}, B = \frac{Ka}{mc}$, non-dimensional parameters; **h,** tube in dimensionless form; $\varphi = \frac{b}{a}$, amplitude proportion.

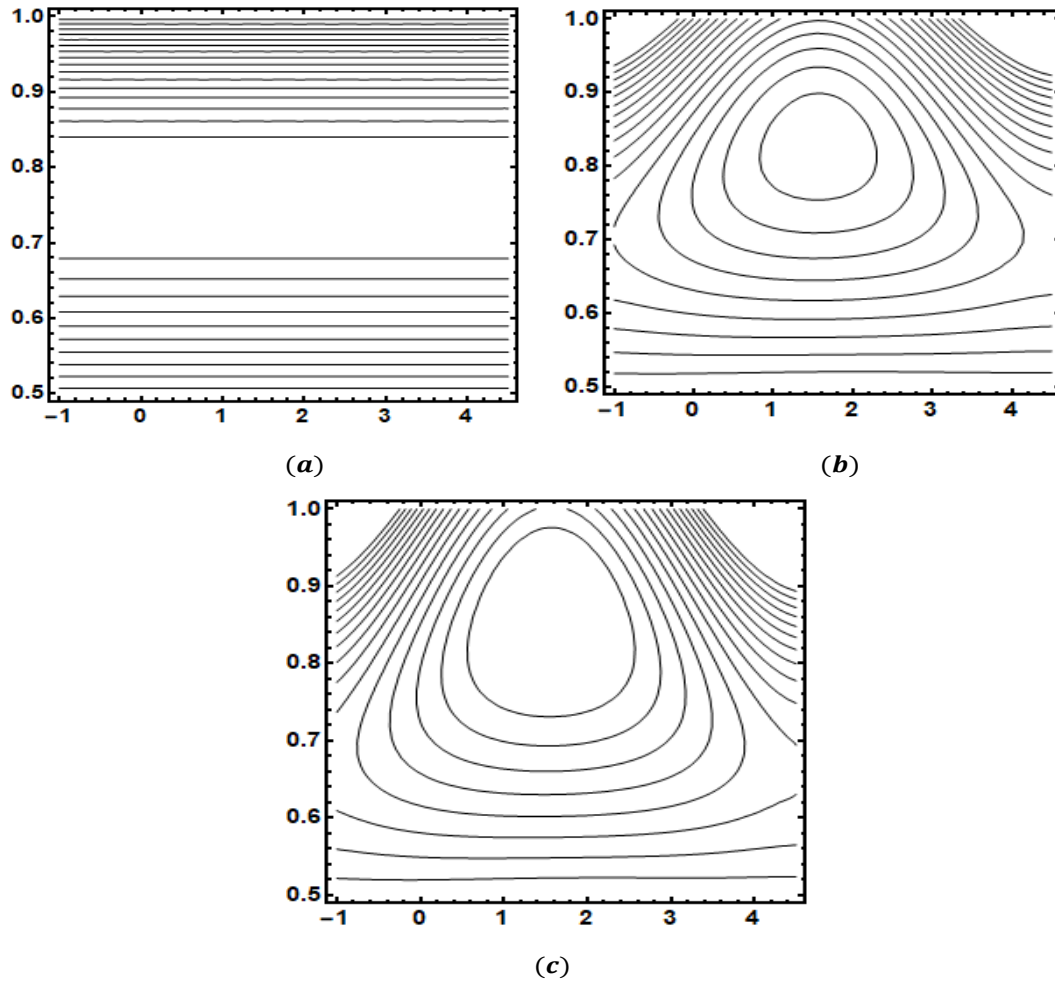**Figure 22.** Streamline presentation of solid grains for $(a)\ \varphi = 0\ (b)\ \varphi = 0.1\ (c)\ \varphi = 0.15$ with $Q_s = 0.6, \alpha = 1.5, A = 1, B = 2, \delta = 0.05, Q = 0.6\ and\ Re = 5.$
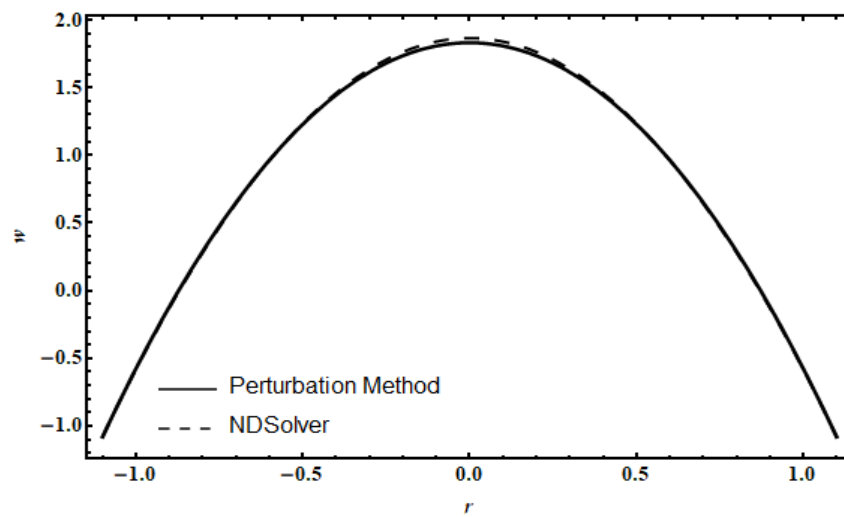
Figure 23. Comparison between perturbation method and numerical method with $\varphi = 0.15, Q_s = 0.6, \alpha = 0.5, A = 1, B = 2, \delta = 0.02, Q = 0.6,\ and\ Re = 5.$

CONFLICT OF INTERESTS

The authors have not declared any conflict of interests.

REFERENCES

Ali N, Asghar Z, Sajid M, Abbas F (2019a). A hybrid numerical study of bacteria gliding on a shear rate-dependent slime." Physica *A: Statistical Mechanics and its Applications* 535:122435.

Ali N, Asghar Z, Sajid M, Bég OA (2019b). Biological interactions between Carreau fluid and microswimmers in a complex wavy canal with MHD effects. Journal of the Brazilian Society of Mechanical Sciences and Engineering 41(10):446

Asghar Z, Ali N (2019a). A mathematical model of the locomotion of bacteria near an inclined solid substrate: effects of different waveforms and rheological properties of couple-stress slime," Canadian Journal of Physics 97(5):537-547.

Asghar Z, Ali N, Ahmed R, Waqas M, Khan WA (2019b). "A mathematical framework for peristaltic flow analysis of non-Newtonian Sisko fluid in an undulating porous curved channel with heat and mass transfer effects," Computer methods and programs in biomedicine 182:105040.

Asghar Z, Ali N, Javid K, Waqas M, Dogonchi AS, Khan WA. (2020b). Bio-Inspired Propulsion of Micro-Swimmers Within A Passive Cervix Filled With Couple Stress Mucus. Computer Methods and Programs in Biomedicine 189:105313.

Asghar Z, Ali N, Sajid M (2018). "Mechanical effects of complex rheological liquid on a microorganism propelling through a rigid cervical canal: swimming at low Reynolds number," Journal of the Brazilian Society of Mechanical Sciences and Engineering 40(9):475.

Asghar Z, Ali N, Sajid M (2019a). Analytical and numerical study of creeping flow generated by active spermatozoa bounded within a declined passive tract. The European Physical Journal Plus 134(1):1-15.

Asghar Z, Ali N, Sajid M, Bég OA (2019b). Magnetic microswimmers propelling through biorheological liquid bounded within an active channel. Journal of Magnetism and Magnetic Materials 486:165283.

Asghar Z, Ali N, Waqas M, Javed MA (2019c). An implicit finite difference analysis of magnetic swimmers propelling through non-Newtonian liquid in a complex wavy channel. Computers & Mathematics with Applications 79(8):2189-2202.

Asghar Z, Javid K, Waqas M, Ghaffari A, Khan WA (2020a). "Cilia-driven fluid flow in a curved channel: Effects of complex wave and porous medium. Fluid Dynamics Research 52(1):015514.

Bhatti MM, Zeeshan A, Ijaz N, Bég OA, Kadir A (2017). Mathematical modelling of nonlinear thermal radiation effects on EMHD peristaltic pumping of viscoelastic dusty fluid through a porous medium duct. Engineering science and technology, an international journal 20(3):1129-1139.

Dogonchi AS, Asghar Z, Waqas M (2020). CVFEM simulation for Fe3O4-H2O nanofluid in an annulus between two triangular enclosures subjected to magnetic field and thermal radiation," International Communications in Heat and Mass Transfer 112:104449.

Hameed M, Khan AA., Ellahi R, Raza M (2015). "Study of magnetic and heat transfer on the peristaltic transport of a fractional second grade fluid in a vertical tube," Engineering Science and Technology, an International Journal 18(3):496-502.

Hayat T Khan MI, Khan TA, Khan MI, Ahmad S, Alsaedi A (2018). Entropy generation in Darcy-Forchheimer bidirectional flow of water-based carbon nanotubes with convective boundary conditions. Journal of Molecular Liquids 265:629-638.

Hayat T, Khan MI, Alsaedi A, Khan MI (2017b). Joule heating and viscous dissipation in flow of nanomaterial by a rotating disk. International Communications in Heat and Mass Transfer 89:190-197.

Hayat T, Khan MI, Farooq M, Alsaedi A, Waqas M, Yasmeen (2016a). T "Impact of Cattaneo–Christov heat flux model in flow of variable thermal conductivity fluid over a variable thicked surface. International Journal of Heat and Mass Transfer 99:702-710.

Hayat T, Khan MI, Farooq M, Yasmeen T, Alsaedi A (2016b). Stagnation point flow with Cattaneo-Christov heat flux and homogeneous-heterogeneous reactions. Journal of Molecular Liquids 220:49-55.

Hayat T, Khan MI, Qayyum S, Alsaedi A (2018a). Entropy generation in flow with silver and copper nanoparticles Colloids and Surfaces A: Physicochemical and Engineering Aspects 539:335-346

Hayat T, Khan MI, Waqas M, Alsaedi A, Farooq M (2017a). Numerical simulation for melting heat transfer and radiation effects in stagnation point flow of carbon–water nanofluid, Computer methods in applied mechanics and engineering 315:1011-1024.

Hayat T, Khan SA, Khan MI, Alsaedi A (2019). Theoretical investigation of Ree–Eyring nanofluid flow with entropy optimization and Arrhenius activation energy between two rotating disks. Computer methods and programs in biomedicine 177:57-68.

Hayat T, Qayyum S, Khan MI, Alsaedi A (2017c). "Current progresses about probable error and statistical declaration for radiative two-phase flow using AgH2O and CuH2O nanomaterials, International Journal of Hydrogen Energy 42(49):29107-29120.

Hayat T, Rafiq M, Alsaedi A, Ahmad B (2014). Radiative and Joule heating effects on peristaltic transport of dusty fluid in a channel with wall properties. The European Physical Journal Plus 129(10):225.

Javid K, Ali N, Asghar Z (2019a). Numerical simulation of the peristaltic motion of a viscous fluid through a complex wavy non-uniform channel with magnetohydrodynamic effects. Physica Scripta 94(11):115226.

Javid K, Ali N, Asghar Z (2019b). "Rheological and magnetic effects on a fluid flow in a curved channel with different peristaltic wave profiles," Journal of the Brazilian Society of Mechanical Sciences and Engineering 41(11):483.

Khan AA, Tariq H (2018). Influence of wall properties on the peristaltic flow of a dusty Walter's B fluid," Journal of the Brazilian Society of Mechanical Sciences and Engineering 40(8):368.

Khan MI, Kumar A, Hayat T, Waqas M, Singh R (2019). Entropy generation in flow of Carreau nanofluid. Journal of Molecular Liquids, 278:677-687.

Khan MI, Qayyum S, Hayat T, Khan MI, Alsaedi A, Khan T (2018b). Entropy generation in radiative motion of tangent hyperbolic nanofluid in presence of activation energy and nonlinear mixed convection," Physics Letters A, 382(31):2017-2026.

Khan MI, Waqas M, Hayat T, Alsaedi A (2017). A comparative study of Casson fluid with homogeneous-heterogeneous reactions, Journal of colloid and interface science 498:85-90.

Khan MWA, Khan MI, Hayat T, Alsaedi A (2018a). "Entropy generation minimization (EGM) of nanofluid flow by a thin moving needle with nonlinear thermal radiation," Physica B: Condensed Matter 534:113-119.

Kumar NS (1980). Flow of a Dusty Fluid Past a Wavy Noving Wall. Journal of the Physical Society of Japan 49(1):391-395.

Morgan GW, Kiely JP (1957). Wave propagation in a viscous liquid contained in a flexible tube. The Journal of the Acoustical Society of America 26(3):323-328.

Olsen JH, Shapiro AH (1967). Large-amplitude unsteady flow in liquid-filled elastic tubes. Journal of Fluid Mechanics 29:513-538.

Pandey SK, Chaube MK (2010). Peristaltic transport of a visco-elastic fluid in a tube of non-uniform cross section," Mathematical and Computer Modelling 52(3-4):501-514.

Pantokratoras A (2018). "Flow past a rotating sphere in a non-Newtonian, power-law fluid, up to a Reynolds number of 10,000," Chemical Engineering Science 181:311-314.

Qayyum S, Hayat T, Khan MI, Khan MI, Alsaedi A (2018b). Optimization of entropy generation and dissipative nonlinear radiative Von Karman's swirling flow with Soret and Dufour effects. Journal of Molecular Liquids 262:261-274.

Qayyum S, Khan MI, Hayat T, Alsaedi A, Tamoor M (2018a). Entropy generation in dissipative flow of Williamson fluid between two rotating disks. International Journal of Heat and Mass Transfer 127:933-942.

Rashid M, Khan MI, Hayat T, Khan MI, Alsaedi (2019). A Entropy generation in flow of ferromagnetic liquid with nonlinear radiation and slip condition. Journal of Molecular Liquids 276:441-452.

Rathod VP, Kulkarni P (2011). The influence of wall properties on peristaltic transport of Dusty fluid through porous medium,"

International Journal of Mathematical Archive 2(12):2229-5046.

Saffman PG (1962). "On the stability of laminar flow of a dusty gas. Journal of fluid mechanics 13(1):120-128.

Shaheen A, Asjad MI (2018). Peristaltic flow of a Sisko fluid over a convectively heated surface with viscous dissipation. Journal of Physics and Chemistry of Solids 122:210-217.

Siddiqui AM, Schwarz WH (1994). Peristaltic flow of a second-order fluid in tubes. Journal of Non-Newtonian Fluid Mechanics 53:257-284.

Singh BK, Singh UP (2014). "Analysis of Peristaltic Flow in a Tube: Rabinowitsch Fluid Model International Journal of Fluids Engineering 6:1-8.

Streeter VL, Keitzer WF, Bohr DF (1964). "Energy dissipation in pulsatile flow through distensible tapered vessels," Pulsatile blood flow, pp. 149-177 McGraw-Hill New York.

Womersley JR (1957). An elastic tube theory of pulse transmission and oscillatory flow in mammalian arteries. WADC Technical report, pp. 56-614.

Yin F, Fung YC (1969). "Peristaltic waves in circular cylindrical tubes," Journal of Applied Mechanics 36:579-587.